AIAA JOURNAL
Vol. 42, No. 6, June 2004

Multimode Decomposition in Compressible Boundary Layers

Paul Gaydos* and Anatoli Tumin†
University of Arizona, Tucson, Arizona 85721

Two-dimensional spatially growing perturbations in a two-dimensional compressible boundary layer are considered within the scope of linearized Navier–Stokes equations in a quasi-parallel flow approximation. Because a spatially growing solution can be expanded into a biorthogonal eigenfunction system, the latter can be utilized for decomposition of flowfields derived from computational studies when pressure, temperature, and all velocity components, together with their derivatives, are available. The method can be used also in a case where partial data are available when a priori information leads to consideration of a finite number of modes.

Nomenclature

$\boldsymbol{A}(x, y, t)$	=	vector function of nine components
A_j	=	jth component of vector $\boldsymbol{A}$
D	=	d/dy
H^{ij}, L^{ij}	=	ij-matrix element
M	=	local Mach number
m	=	$2(e-1)/3$
Pr	=	Prandtl number
p	=	Laplace variable
R	=	Reynolds number
r	=	$2(e+2)/3$
T_s	=	mean flow temperature
U_s	=	mean flow velocity
u	=	streamwise velocity disturbance
v	=	normal velocity disturbance
x	=	streamwise coordinate
y	=	coordinate normal to the wall
α	=	streamwise wave number
γ	=	specific heat ratio
θ	=	temperature disturbance
μ	=	viscosity disturbance
μ_s	=	mean flow viscosity
μ_s'	=	$\mathrm{d}\mu_s/\mathrm{d}T_s$
π	=	pressure disturbance
ρ	=	density disturbance
ρ_s	=	mean flow density
$2e/3$	=	ratio of the bulk viscosity to the dynamic viscosity

Subscripts

e	=	edge of the boundary layer
s	=	mean flow

Superscript

T	=	transposed

Introduction

THE progress being made in computational fluid dynamics (CFD) provides an opportunity for reliable simulation of such complex phenomenon as laminar–turbulent transition. The dynamics of flow transition depends on the instability of small perturbations excited by external sources. CFD provides complete information about the flowfield, which would be impossible to measure in real experiments. However, this increase in available information does not furnish a physical insight of the transition because the leading mechanisms still remain hidden behind a messy disturbance field. Sometimes, a flow possesses a few instability modes that are equally significant in the transition process, and it might be desirable to distinguish the dynamics of each mode in the complex nonsteady flowfield. Figure 1 illustrates the dependence of the real parts of wave numbers of the first and the second discrete modes on the local Reynolds number, $R = \sqrt{(\rho_e U x/\mu_e)}$, in a hypersonic boundary layer over a sharp cone, where ρ_e, μ_e, and U_e are density, viscosity, and mean velocity at the edge of the boundary layer. The coordinate x is measured along the surface of the cone, and the wave numbers are dimensionless with the help of the length scale $\sqrt{(\mu_e x/\rho_e U_e)}$. In this example and what follows, the boundary-layer solution was obtained with Mangler transformation from a planar to a conical configuration. The frequency parameter is $F = 150 \times 10^{-6}$, and the Mach number is equal to 5.6. One can see that there is a synchronism of these two modes in the vicinity of $R = 1600$. The synchronism is not absolute because the eigenvalues α have small but different imaginary parts. Nevertheless, the complex wave numbers are very close, and Fig. 2 demonstrates that the mode shapes are very close as well. In simple words, one has to recognize these modes in the presence of acoustic, vorticity, and entropy modes and separate them from one another. Consequently, the problem of decomposing the flowfields into normal modes arises. Because CFD provides complete information about the flowfield, one can expect that the decomposition may be formulated as a rigorous procedure.

We shall discuss the problem of two-dimensional perturbations in two-dimensional compressible boundary layers. The linearized Navier–Stokes equations are considered the governing equations for the perturbations, and they provide the basis for the decomposition. Gustavsson[1] solved a temporal initial-value problem in a parallel boundary layer by using Fourier–Laplace transforms. The inverse Laplace transform was presented as a sum of integrals along a branch cut (continuous spectrum) and the residue values at poles (discrete spectrum). Salwen and Grosch[2] formulated a biorthogonal eigenfunction system within the scope of a temporal stability theory and derived an orthogonality condition between the eigenfunctions of the direct and adjoint linearized equations. They also showed that the results in Ref. 1 can be recast as an expansion of the solution into the eigenfunctions of continuous and discrete spectra, with coefficients depending on the initial perturbation. The results in Ref. 2 can be used for decomposition of, for example, wave packets in boundary layers. Later, Fedorov and Tumin[3] extended the analysis of the temporal initial-value problem to compressible boundary-layer flows.

Another class of problems is associated with spatially growing perturbations in boundary-layer flows. The signaling problem may serve as an example.[4,5] This problem is related to a disturbance generator of prescribed frequency starting oscillations at initial time

Received 6 May 2003; presented as Paper 2003-3724 at the AIAA 33rd Fluid Dynamics Conference, Orlando, FL, 23–26 June 2003; revision received 18 January 2004; accepted for publication 4 March 2004.

*Research Assistant, Department of Aerospace and Mechanical Engineering.

†Associate Professor, Department of Aerospace and Mechanical Engineering; tumin@engr.arizona.edu. Senior Member AIAA.

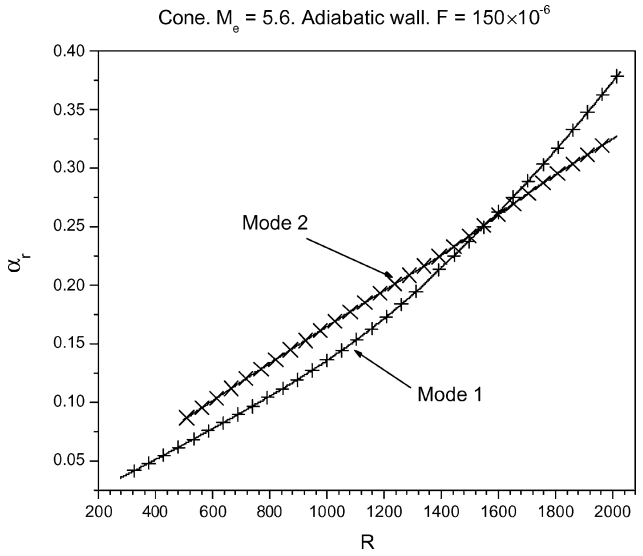

Fig. 1 Wave numbers of two discrete modes.

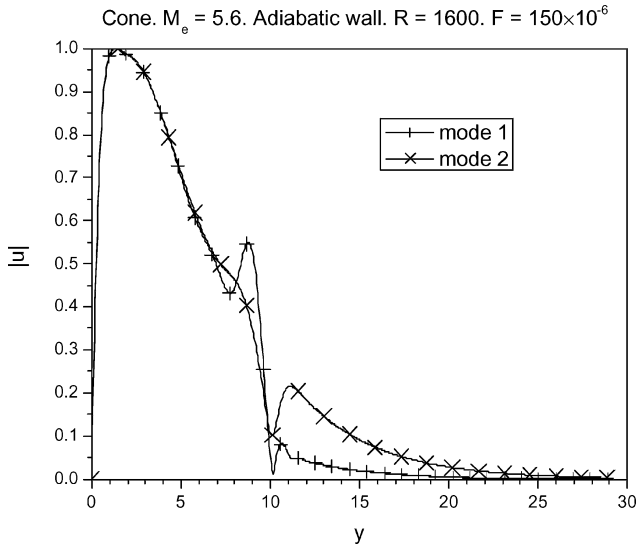

Fig. 2 Profiles (normalized to 1) of the discrete modes at $R = 1600$. Eigenvalues of the first and the second modes are $\alpha_1 = 0.2627 + i0.02269$ and $\alpha_2 = 0.2603 - i0.00494$, respectively.

$t = 0$. After a transient period of time, the solution of the linearized Navier–Stokes equations may be expressed as a sum of integrals along branch cuts (continuous spectrum) and the residue values at poles (discrete spectrum) in the complex wave number plane. The corresponding biorthogonal eigenfunction system for spatially growing disturbances was introduced independently by Zhigulev et al.[6] and by Salwen and Grosch[2] for two-dimensional perturbations in two-dimensional incompressible boundary layers. In addition to discrete modes (Tollmien–Schlichting-like modes), there are four branches of continuous spectra. The modes of two branches have arbitrary large growth rates in the downstream direction. This indicates that a spatial initial-value problem is ill posed, and Hadamard's example[7] illustrates the ill-posedness of the problem. The ill-posedness was a stumbling block in the decomposition of spatially growing disturbances into modes because the method in Refs. 1 and 2 could not be applied. However, the ill-posedness was recognized by Tumin and Fedorov[8] (see also Ref. 9), and a suggestion was made to consider spatial initial-value problems when the solution has a finite growth rate in the downstream direction. An analysis of compressible[8] and incompressible boundary layers[9] using a Laplace transform with respect to the streaming coordinate x demonstrated completeness of the biorthogonal eigenfunction system, similar to the temporal theory.[1,2]

The results in Ref. 9 could be used for decomposition of CFD data when pressure, temperature, and disturbance perturbations, velocity disturbance profiles, and their streamwise derivatives are known at one station, x. In experiments, one usually deals with partial information; that is, only one velocity component is measured. If, for some reason, one can expect that only a few modes are responsible for the total signal measured in the experiment, this a priori information also can be helpful to decompose the experimental flowfield. The first application of multimode decomposition was carried out for an analysis of experimental data in a laminar wall jet when only one velocity component was measured.[10] The main feature of the laminar wall jet is that two unstable discrete modes can coexist in the flow. This allowed the assumption that these two modes provide the main input into the measured signal somewhere far downstream from a vibrating ribbon. Therefore, the decomposition becomes possible with the help of one velocity component measured at a downstream station. Comparison of recovered and measured data illustrated good agreement. Later on, the method was applied to an analysis of numerical results for forced transitional wall jets.[11] Recently, the method was extended to three-dimensional perturbations in an incompressible boundary layer.[12]

The objective of the present work is to discuss/illustrate the possible application of the biorthogonal eigenfunction system to the multimode decomposition of direct numerical simulation and experimental data in case of compressible boundary layers.

Governing Equations and Formal Solution to the Spatial Cauchy Problem

We analyze two-dimensional perturbations in a two-dimensional compressible boundary layer, and the boundary layer is considered in the parallel flow approximation. After Fourier transform with respect to time, the linearized Navier–Stokes equations are recast in the following matrix form:

$$\frac{\partial}{\partial y}\left(L_0\frac{\partial \boldsymbol{A}}{\partial y}\right) + L_1\frac{\partial \boldsymbol{A}}{\partial y} = H_1\boldsymbol{A} + H_2\frac{\partial \boldsymbol{A}}{\partial x} \tag{1}$$

where L_0, L_1, H_1, and H_2 are 9×9 matrices. Their nonzero elements are presented in Appendix A. The vector function $\boldsymbol{A}(x, y)$ is defined with the help of the streamwise and normal velocity perturbations, u and v, respectively; pressure perturbation π; and temperature perturbation θ:

$$\boldsymbol{A} = \left(u, \frac{\partial u}{\partial y}, v, \pi, \theta, \frac{\partial \theta}{\partial y}, \frac{\partial u}{\partial x}, \frac{\partial v}{\partial x}, \frac{\partial \theta}{\partial x}\right)^T \tag{2}$$

The boundary conditions are a no-slip condition on the wall and decaying perturbations outside the boundary layer.

For the purpose of clarity, we briefly recapitulate the main ideas of Ref. 8. The Cauchy problem for Eq. (1) with initial data at $x = 0$ is ill posed. The latter is associated with possible upstream influence of the downstream boundary of the domain. However, if there is no evidence of the upstream impact, one can assume that the solution has a finite growth rate along the coordinate x.

Assuming that the solution has a finite growth rate, we apply the Laplace transform with respect to x:

$$\boldsymbol{A}_p(y) = \int_0^\infty \boldsymbol{A}(x, y)e^{-px}\,\mathrm{d}x \tag{3}$$

As a result, we arrive at the following inhomogeneous system of ordinary differential equations:

$$\frac{\mathrm{d}}{\mathrm{d}y}\left(L_0\frac{\mathrm{d}\boldsymbol{A}_p}{\mathrm{d}y}\right) + L_1\frac{\mathrm{d}\boldsymbol{A}_p}{\mathrm{d}y} - H_1\boldsymbol{A}_p - pH_2\boldsymbol{A}_p = \boldsymbol{F} \tag{4}$$

$$\boldsymbol{F} = -H_2\boldsymbol{A}_0$$

where the vector function $\boldsymbol{A}_0$ stands for the initial data at $x=0$. A homogeneous system of equations corresponding to Eqs. (4) can be recast in the form

$$\frac{\mathrm{d}z}{\mathrm{d}y} = H_0 z \tag{5}$$

where H_0 is a 6×6 matrix (see Appendix A) and z is a vector function composed of the first six elements of vector function $\boldsymbol{A}_p$. The system of equations (5) has six fundamental solutions, $z_1(y), z_2(y), \ldots, z_6(y)$. Because their properties will be used in further analysis, we shall discuss them in detail.

Classification of the fundamental solutions stems from their behavior outside the boundary layer, where $U_s(y)\equiv 1$, $T_s(y)\equiv 1$, and derivatives of the mean flow profiles are equal to zero. Solutions of Eq. (5) outside the boundary layer have an exponential form as $z_j^0 \exp(\lambda_j y)$. For $y\to\infty$, the characteristic equation

$$\det\|H_0 - \lambda \boldsymbol{I}\| = 0 \tag{6}$$

can be written in the explicit form

$$\begin{gathered}\left(b_{11}-\lambda^2\right)\times\left[\left(b_{22}-\lambda^2\right)\left(b_{33}-\lambda^2\right)-b_{23}b_{32}\right]=0\\ b_{11}=H_0^{21},\qquad b_{22}=H_0^{42}H_0^{24}+H_0^{43}H_0^{34}+H_0^{46}H_0^{64}\\ b_{23}=H_0^{42}H_0^{25}+H_0^{43}H_0^{35}+H_0^{46}H_0^{65}\\ b_{32}=H_0^{64},\qquad b_{33}=H_0^{65}\end{gathered} \tag{7}$$

where elements of matrix H_0 are evaluated at $y\to\infty$. The roots of Eq. (7) are

$$\begin{gathered}\lambda_{1,2}^2 = b_{11} = \alpha^2 + iR(\alpha-\omega)\\ \lambda_{3,4}^2 = [(b_{22}+b_{33})/2] - \tfrac{1}{2}\sqrt{(b_{22}-b_{33})^2+4b_{23}b_{32}}\\ \lambda_{5,6}^2 = [(b_{22}+b_{33})/2] + \tfrac{1}{2}\sqrt{(b_{22}-b_{33})^2+4b_{23}b_{32}}\end{gathered} \tag{8}$$

Solution of the inhomogeneous system of differential equations (4) can be expressed in terms of the fundamental solutions $z_1(y), z_2(y), \ldots, z_6(y)$ with coefficients depending on the initial data $\boldsymbol{A}_0$. The inverse Laplace transform could be presented as a sum of residue values at poles corresponding to the modes of discrete spectrum and a sum of integrals along branch cuts in the complex plane p. These branch cuts are associated with the continuous spectrum, and they can be found from

$$\lambda_j^2 = -k^2, \qquad j=1,\ldots,6 \tag{9}$$

where k is a positive parameter. In the case of the spatially growing disturbances, there are seven branches of the continuous spectrum. This number stems from the fact that the characteristic equation represents a polynomial of seventh order with respect to the wave number, $\alpha = ip$. (The continuity equation has the first derivative with respect to x; the two momentum equations and the energy equation have second derivatives with respect to x.) In particular, indices $j=1$ and 2 correspond to the vorticity modes, whereas the others correspond to the acoustic and entropy modes [depending on the branch of the square root in Eq. (8)]. The classification of the modes follows from their properties outside the boundary layer. (One can find discussion of the properties of vorticity, entropy, and acoustic modes in Ref. 13.)

Figure 3 demonstrates branches of the continuous spectrum at local Mach number $M_e = 0.5$ in the complex plane $\alpha = ip$. Figure 4 shows the branches in the case of a supersonic flow ($M_e = 2$). In both examples the dimensionless frequency was chosen equal to 1. The relatively small Reynolds numbers are chosen for purpose of the illustration only. (The Mach numbers on the illustrations are the same as in Ref. 8.) One can see that there are three modes with negative imaginary parts of α. They are associated with upstream perturbations. The other four modes correspond to the downstream modes. One of the branches has a limiting point as parameter k tends to infinity. Although the limiting point exists at significantly high positive values of α_i that are usually not of interest, we demonstrate the structure of the branches for completeness of the illustration. The branches can be interpreted as acoustic, entropy, and vorticity modes in accordance with their properties outside the boundary layer. Note that the branch having a limiting point in the upper half-plane was calculated incorrectly in Ref. 8. The correct behavior of this branch was found by D. E. Ashpis (private communication, 1993). However, the error was associated with strongly decaying modes, and it did not affect the main result and conclusions of Ref. 8.

Biorthogonal Eigenfunction System

It was shown in Ref. 8 that the formal solution of the spatial initial-value problem could be represented as a sum of the continuous and discrete spectra. The direct and the adjoint problems corresponding to these modes ($\boldsymbol{A}_\alpha$ and $\boldsymbol{B}_\alpha$, respectively) are the following:

$$\begin{cases}\dfrac{\mathrm{d}}{\mathrm{d}y}\left(L_0\dfrac{\mathrm{d}\boldsymbol{A}_\alpha}{\mathrm{d}y}\right)+L_1\dfrac{\mathrm{d}\boldsymbol{A}_\alpha}{\mathrm{d}y}=H_1\boldsymbol{A}_\alpha+i\alpha H_2\boldsymbol{A}_\alpha\\ y=0:\quad A_{\alpha 1}=A_{\alpha 3}=A_{\alpha 5}=0\\ y\to\infty:\quad |A_{\alpha j}|<\infty\end{cases} \tag{10}$$

$$\begin{cases}\dfrac{\mathrm{d}}{\mathrm{d}y}\left(L_0^T\dfrac{\mathrm{d}\boldsymbol{B}_\alpha}{\mathrm{d}y}\right)-L_1^T\dfrac{\mathrm{d}\boldsymbol{B}_\alpha}{\mathrm{d}y}=H_1^T\boldsymbol{B}_\alpha+i\alpha H_2^T\boldsymbol{B}_\alpha\\ y=0:\quad B_{\alpha 2}=B_{\alpha 4}=B_{\alpha 6}=0\\ y\to\infty:\quad |B_{\alpha j}|<\infty\end{cases} \tag{11}$$

In the definition of the adjoint problem, we do not introduce the complex conjugate due to the convenience associated with a numerical realization. The subscript α indicates that the mode is associated with the wave number.

The system of equations (10) can be recast in the form of Eq. (5), whereas Eq. (11) can be recast as

$$-\frac{\mathrm{d}\boldsymbol{Y}}{\mathrm{d}y} = H_0^T\boldsymbol{Y} \tag{12}$$

We have found relationships between components of vectors $\boldsymbol{B}$ and $\boldsymbol{Y}$ with the help of Mathematica[14] (see Appendix B).

The following orthogonality condition exists:

$$\langle H_2\boldsymbol{A}_\alpha, \boldsymbol{B}_{\alpha'}\rangle \equiv \sum_{j=1}^{9}\int_0^\infty (H_2\boldsymbol{A}_\alpha)_j B_{\alpha' j}\,\mathrm{d}y = Q\Delta_{\alpha,\alpha'} \tag{13}$$

where $\Delta_{\alpha,\alpha'}$ is the Kronecker symbol if α or α' belongs to the discrete spectrum, and $\Delta_{\alpha,\alpha'}=\delta(\alpha-\alpha')$ is the delta function if both α and α' belong to the continuous spectrum. The coefficient Q on the right-hand side of relation (13) depends on normalization of $\boldsymbol{A}_\alpha(y)$ and $\boldsymbol{B}_\alpha(y)$.

If we have a vector function $\boldsymbol{A}_0(y)$ (for example, from a computational study), we can find the amplitude of a mode as follows:

$$C_\alpha = \frac{\langle H_2\boldsymbol{A}_0, \boldsymbol{B}_\alpha\rangle}{\langle H_2\boldsymbol{A}_\alpha, \boldsymbol{B}_\alpha\rangle} \tag{14}$$

An example of two discrete modes is given in Fig. 2. Examples of the acoustic modes in the boundary layer over a cone $R=1600$ and $F=150\times 10^{-6}$ are shown in Fig. 5. The parameter k in these examples is equal to 1 and the normalization of the modes was defined by the equation $\partial u/\partial y = 1$ on the wall.

Examples of the Multimode Decomposition

We consider two examples. The first one is an emulation of the analysis of a flowfield obtained by means of a computational method; that is, all parameters of the flow are assumed to be known at a prescribed station x. The second example will be an emulation of

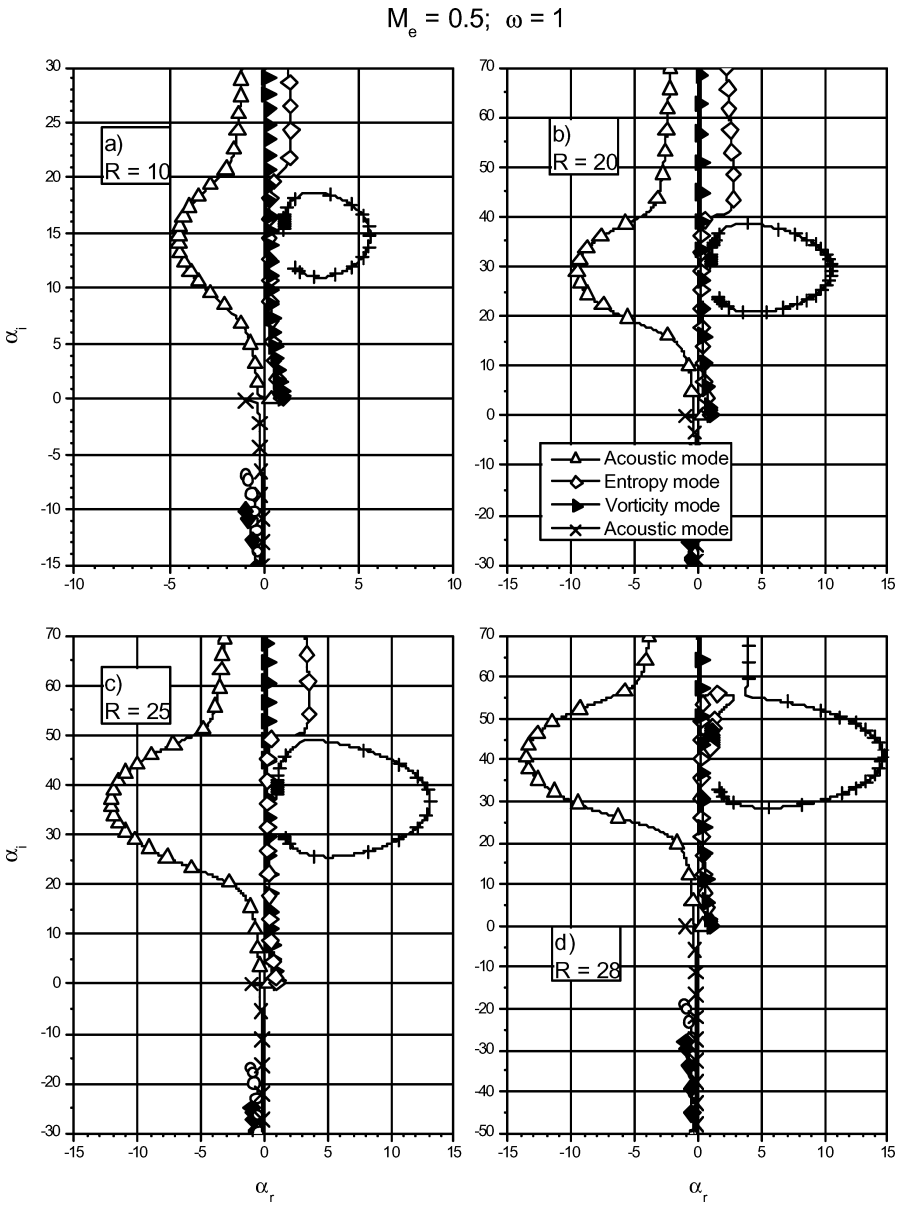

Fig. 3 Branches of the continuous spectrum in the complex plane α.

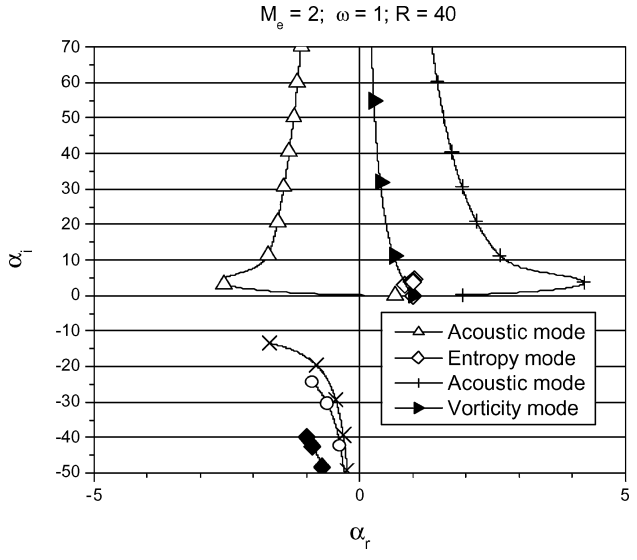

Fig. 4 Branches of the continuous spectrum in the complex plane α.

the decomposition of "experimental" data. Details of the numerical methods are presented in Ref. 3.

CFD Flowfield

Figure 6 gives an example of a flowfield, $A_0(y)$, composed of two discrete modes (Fig. 2) with amplitudes $C_1 = 1$ and $C_2 = -1$, acoustic and vorticity modes, respectively. The sum of the discrete modes only is shown in Fig. 7. It is very difficult to imagine the presence of the discrete modes in the total flowfield. The phase shift between the modes was chosen to illustrate how interpretation of the flowfield might be complicated. The decomposition procedure, Eq. (14), leads to the coefficients $C_1 = 1.0018 + i\,1.58e{-}03$ and $C_2 = -0.9997 - i\,1.59e{-}04$. The negligible discrepancy with the actual values is attributed to the accuracy of the numerical evaluation of the integrals.

Evaluation of the coefficient Q in Eq. (13) in the case of the discrete spectrum is straightforward: numerical integration on the interval $[0, y_{\max}]$ and analytical calculation on the interval $[y_{\max}, \infty)$. In the case of the continuous spectra, the coefficient Q can be found with the help of the asymptotic solutions outside of the boundary layer. An outline of the evaluation is given in Ref. 12. We would

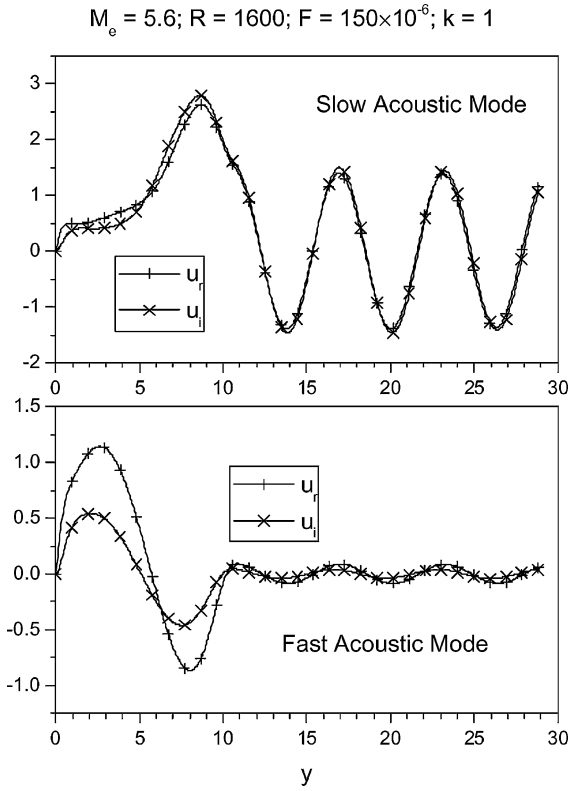

Fig. 5 Streamwise velocity component of acoustic modes.

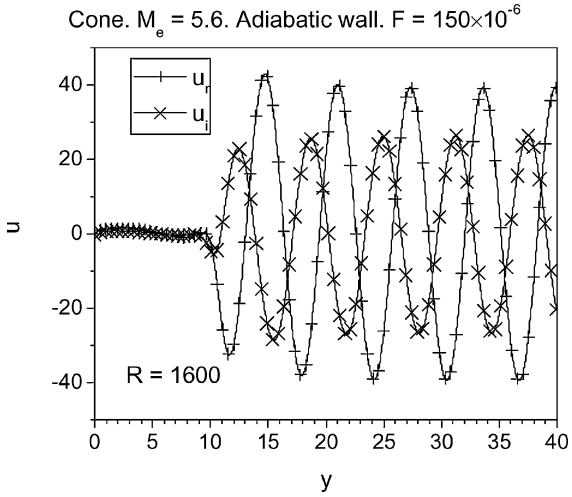

Fig. 6 Real and imaginary parts of the combined flowfield (two discrete modes, vorticity and acoustic).

like to point out that the coefficient Q and, therefore, coefficients C_j depend on the normalization of the biorthogonal eigenfunction system. However, the product of the coefficients and the eigenfunctions $\boldsymbol{A}_\alpha$ is invariant with respect to the normalization.

Experimental Flowfield

In the previous example, all components of the vector $\boldsymbol{A}_0(y)$ were known. If, for some reason, one can expect that only a few modes are responsible for the total signal measured in the experiment, this a priori information also can be helpful in decomposing the experimental flowfield. The assumption about the main input from specific modes actually allows recovery of the other components in the vector $\boldsymbol{A}_0(y)$ with unknown coefficients. For example, we have "experimental" data for the x velocity component as in Figs. 8 and 9 (amplitude and phase of the streamwise velocity perturbation corresponding to Fig. 7). If there is a priori information that the data

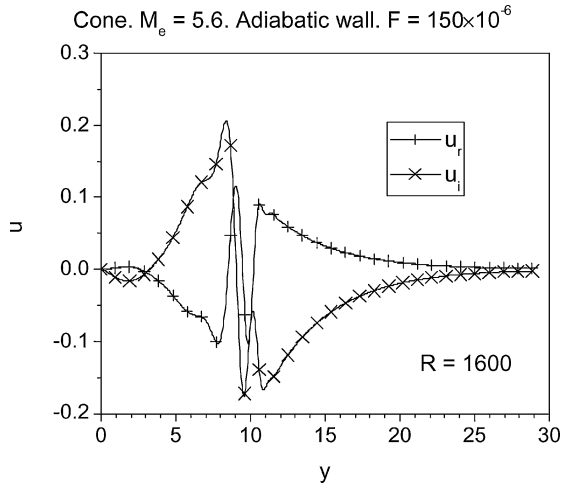

Fig. 7 Real and imaginary parts of the combined flowfield (two discrete modes only). Compare magnitudes of the functions in Figs. 6 and 7.

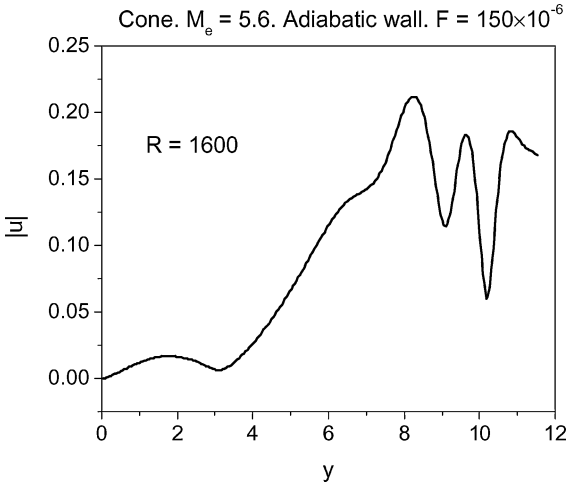

Fig. 8 Experimental streamwise velocity disturbance amplitude distribution across the boundary layer.

comprise two discrete modes associated with wave numbers α_1 and α_2, one can represent the vector $\boldsymbol{A}_0(y)$ as follows:

$$A_0(y) = \big(u, C_1A_{\alpha_1} + C_2A_{\alpha_21}, C_1A_{\alpha_12} + C_2A_{\alpha_22},$$
$$C_1A_{\alpha_13} + C_2A_{\alpha_23}, C_1A_{\alpha_14} + C_2A_{\alpha_24}, C_1A_{\alpha_15} + C_2A_{\alpha_25},$$
$$C_1A_{\alpha_16} + C_2A_{\alpha_26}, C_1A_{\alpha_17} + C_2A_{\alpha_27}, C_1A_{\alpha_18} + C_2A_{\alpha_28},$$
$$C_1A_{\alpha_19} + C_2A_{\alpha_29}\big) \tag{15}$$

where $A_{\alpha_j m}$ stands for the mth component of the vector $\boldsymbol{A}_{\alpha_j}$. At the same time, the a priori information suggests that the vector $\boldsymbol{A}_0(y)$ can be represented also as a sum of these two modes:

$$\boldsymbol{A}_0(y) = C_1\boldsymbol{A}_{\alpha_1}(y) + C_2\boldsymbol{A}_{\alpha_2}(y) \tag{16}$$

From the orthogonality condition, one can obtain

$$\langle H_2\boldsymbol{A}_0, \boldsymbol{B}_{\alpha_1}\rangle = C_1\langle H_2\boldsymbol{A}_{\alpha_1}, \boldsymbol{B}_{\alpha_1}\rangle$$
$$\langle H_2\boldsymbol{A}_0, \boldsymbol{B}_{\alpha_2}\rangle = C_2\langle H_2\boldsymbol{A}_{\alpha_2}, \boldsymbol{B}_{\alpha_2}\rangle \tag{17}$$

Substitution of $\boldsymbol{A}_0(y)$ from Eq. (15) into Eq. (17) leads to a system of algebraic equations for C_1 and C_2. This decomposition procedure has been applied to data in Figs. 8 and 9 and the coefficients C_1 and C_2 were found as $1.00002+i1.16e{-}04$ and $-0.999996+i1.65e{-}06$, respectively. Because the experimental data might be contaminated by noise or by other modes that were

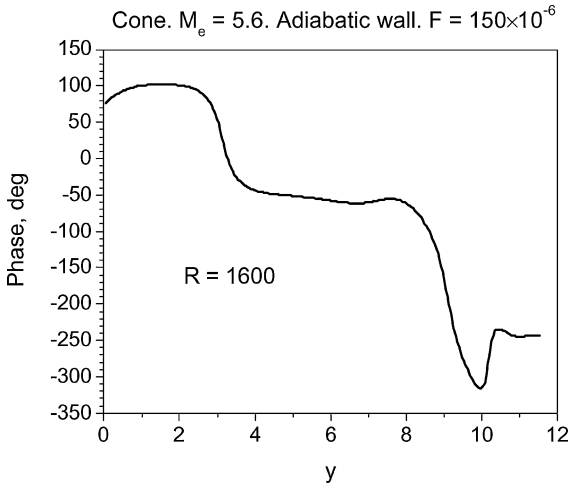

Fig. 9 Experimental streamwise velocity disturbance phase distribution across the boundary layer.

not included in the decomposition, one has to carry out an a posteriori comparison of the measured and recovered profiles to estimate consistency of the decomposition with the a priori information/assumption.

Conclusions

The formulated method of multimode decomposition might be very helpful for the analysis of computational results related to laminar–turbulent transition in compressible boundary layers. Although the present formulation deals with two-dimensional disturbances and two-dimensional boundary layers, the orthogonality relationship can be easily extended to a general case of three-dimensional perturbations when the boundary-layer flow is independent of the spanwise coordinate (for example, infinite swept wing flow). In this case, the Fourier transform with respect to the spanwise coordinate can be employed and the orthogonality condition can be formulated for the modes having the same spanwise wave number. The method might be also useful in the analysis of real experimental data when a priori information about the modes is available.

Appendix A: Nonzero Elements of the Matrices in Eqs. (1) and (5)

The velocity, temperature, and viscosity are scaled using their values at the upper boundary-layer edge; the pressure is scaled using $\rho_e U_e^2$. Nonzero elements of the matrices in Eq. (1) are as follows:

$$L_0^{43} = -\frac{r\mu_s}{R}, \qquad L_1^{ij} = 1 \qquad i, j = 1, \ldots, 6$$

$$L_1^{28} = (m+1), \qquad H_1^{12} = 1$$

$$H_1^{21} = -\frac{i\omega R}{\mu_s T_s}, \qquad H_1^{22} = -D(\ell_n \mu_s)$$

$$H_1^{23} = \frac{R}{\mu_s T_s} DU_s, \qquad H_1^{25} = -\frac{D(\mu_s' DU_s)}{\mu_s}$$

$$H_1^{26} = -\frac{\mu_s'}{\mu_s} DU_s, \qquad H_1^{33} = \frac{DT_s}{T_s}$$

$$H_1^{34} = i\omega\gamma M_e^2, \qquad H_1^{35} = -\frac{i\omega}{T_s}$$

$$H_1^{43} = \frac{i\omega}{T_s}, \qquad H_1^{56} = 1$$

$$H_1^{63} = -2DU_s Pr(\gamma-1)M_e^2, \qquad H_1^{64} = i\omega\frac{RPr}{\mu_s}(\gamma-1)M_e^2$$

$$H_1^{65} = -\frac{Pr(\gamma-1)M_e^2}{\mu_s}\mu_s'(DU_s)^2 - \frac{D(\mu_s' DT_s)}{\mu_s} - \frac{i\omega RPr}{T_s\mu_s}$$

$$H_1^{66} = -\frac{2\mu_s' DT_s}{\mu_s}$$

$$H_1^{77} = 1, \qquad H_1^{88} = 1, \qquad H_1^{99} = 1$$

$$H_2^{21} = \frac{RU_s}{\mu_s T_s}, \qquad H_2^{23} = -D(\ell_n \mu_s)$$

$$H_2^{24} = \frac{R}{\mu_s}, \qquad H_2^{27} = -r$$

$$H_2^{48} = \frac{\mu_s}{R}, \qquad H_2^{69} = -1$$

$$H_2^{31} = -1, \qquad H_2^{34} = -\gamma M_e^2 U_s, \qquad H_2^{35} = \frac{U_s}{T_s}$$

$$H_2^{41} = \frac{mD\mu_s}{R}, \qquad H_2^{42} = (m+1)\frac{\mu_s}{R}$$

$$H_2^{43} = -\frac{U_s}{T_s}, \qquad H_2^{45} = \frac{\mu_s' DU_s}{R}$$

$$H_2^{62} = -2PrDU_s(\gamma-1)M_e^2$$

$$H_2^{64} = -\frac{RPr}{\mu_s}(\gamma-1)M_e^2 U_s$$

$$H_2^{65} = \frac{RPr}{T_s\mu_s}U_s$$

$$H_2^{71} = -1, \qquad H_2^{83} = -1, \qquad H_2^{95} = -1$$

$$H_0^{12} = H_0^{56} = 1$$

$$H_0^{21} = \alpha^2 + i(\alpha U_s - \omega)R/\mu_s T_s$$

$$H_0^{22} = -\frac{D\mu_s}{\mu_s}$$

$$H_0^{23} = -\frac{i\alpha(m+1)DT_s}{T_s} - \frac{i\alpha D\mu_s}{\mu_s} + \frac{RDU_s}{\mu_s T_s}$$

$$H_0^{24} = \frac{i\alpha R}{\mu_s} - (m+1)\gamma M_e^2\alpha(\alpha U_s - \omega)$$

$$H_0^{25} = \frac{\alpha(m+1)(\alpha U_s - \omega)}{T_s} - \frac{D(\mu_s' DU_s)}{\mu_s}$$

$$H_0^{26} = -\frac{\mu_s' DU_s}{\mu_s}$$

$$H_0^{31} = -i\alpha, \qquad H_0^{33} = \frac{DT_s}{T_s}$$

$$H_0^{34} = -i\gamma M_e^2(\alpha U_s - \omega)$$

$$H_0^{35} = \frac{i(\alpha U_s - \omega)}{T_s}$$

$$\chi = \left[\frac{R}{\mu_s} + ir\gamma M_e^2(\alpha U_s - \omega)\right]^{-1}$$

$$H_0^{41} = -i\alpha\chi\left(\frac{rDT_s}{T_s} + \frac{2D\mu_s}{\mu_s}\right)$$

$$H_0^{42} = -i\alpha\chi$$

$$H_0^{43} = \chi\left[-\alpha^2 - \frac{i(\alpha U_s - \omega)R}{\mu_s T_s} + \frac{rD^2 T_s}{T_s} + \frac{rD\mu_s DT_s}{\mu_s T_s}\right]$$

$$H_0^{44} = -i\chi r\gamma M_e^2\left[\alpha DU_s + (\alpha U_s - \omega)\left(\frac{DT_s}{T_s} + \frac{D\mu_s}{\mu_s}\right)\right]$$

$$H_0^{45} = i\chi\left[\frac{r\alpha DU_s}{T_s} + \frac{\alpha\mu_s' DU_s}{\mu_s} + \frac{r(\alpha U_s - \omega)D\mu_s}{\mu_s T_s}\right]$$

$$H_0^{46} = \frac{ir\chi(\alpha U_s - \omega)}{T_s}$$

$$H_0^{62} = -2(\gamma - 1)M_e^2 PrDU_s$$

$$H_0^{63} = -2i\alpha(\gamma - 1)M_e^2 PrDU_s + \frac{RPrDT_s}{\mu_s T_s}$$

$$H_0^{64} = -\frac{iRPr(\gamma - 1)M_e^2(\alpha U_s - \omega)}{\mu_s}$$

$$H_0^{65} = \alpha^2 + \frac{iRPr(\alpha U_s - \omega)}{\mu_s T_s} - \frac{(\gamma - 1)M_e^2 Pr\mu_s'(DU_s)^2}{\mu_s} - \frac{D^2\mu_s}{\mu_s}$$

$$H_0^{66} = -\frac{2D\mu_s}{\mu_s}$$

Appendix B: Correspondence Between Solutions of the Adjoint Problems, Eqs. (11) and (12)

$$B_1 = Y_1 - \frac{i\alpha r Y_4}{\left[(R/\mu_s) + ir\gamma M_e^2(\alpha U_s - \omega)\right]}$$

$$B_2 = Y_2$$

$$B_3 = -i\alpha(m+1)Y_2 + Y_3 + \frac{rDT_s}{T_s}\frac{Y_4}{\left[(R/\mu_s) + ir\gamma M_e^2(\alpha U_s - \omega)\right]}$$

$$-\frac{r\mu_s}{R}\frac{\mathrm{d}}{\mathrm{d}y}\left\{\left(\frac{Y_4}{\left[1 + i(r\mu_s/R)\gamma M_e^2(\alpha U_s - \omega)\right]}\right\}\right.$$

$$B_4 = \frac{Y_4}{\left[1 + i(r\mu_s/R)\gamma M_e^2(\alpha U_s - \omega)\right]}$$

$$B_5 = Y_5 + \frac{ir(\alpha U_s - \omega)}{T_s}\frac{Y_4}{\left[(R/\mu_s) + ir\gamma M_e^2(\alpha U_s - \omega)\right]}$$

$$B_6 = Y_6, \qquad B_7 = i\alpha r B_2, \qquad B_8 = -(m+1)\frac{dB_2}{dy} - i\alpha H_2 B_4$$

$$B_9 = i\alpha B_6$$

Acknowledgment

This work is supported by the U.S. Air Force Office of Scientific Research.

References

[1]Gustavsson, L. H., "Initial-Value Problem for Boundary Layer Flows," *Physics of Fluids*, Vol. 22, No. 9, 1979, pp. 1602–1605.

[2]Salwen, H., and Grosch, C. E., "The Continuous Spectrum of the Orr-Sommerfeld Equation. Part 2. Eigenfunction Expansion," *Journal of Fluid Mechanics*, Vol. 104, 1981, pp. 445–465.

[3]Fedorov, A., and Tumin, A., "Initial-Value Problem for Hypersonic Boundary-Layer Flows," *AIAA Journal*, Vol. 41, No. 3, 2003, pp. 379–389.

[4]Ashpis, D., and Reshotko, E., "The Vibrating Ribbon Problem Revisited," *Journal of Fluid Mechanics*, Vol. 213, 1990, pp. 513–547.

[5]Huerre, P., and Rossi, M., "Hydrodynamic Instabilities in Open Flows," *Hydrodynamics and Nonlinear Instabilities*, edited by C. Godreche and P. Manneville, Cambridge Univ. Press, Cambridge, England, U.K., 1998, pp. 81–294.

[6]Zhigulev, V. N., Sidorenko, N. V., and Tumin, A. M., "Generation of Instability Waves in a Boundary Layer by External Turbulence," *Journal of Applied Mechanics and Technical Physics*, Vol. 21, No. 6, 1980, pp. 28–34.

[7]Hadamard, J., *Le Problème de Cauchy et les Éuations aux Derives Partielles Linéares Hyprboliques*, Hermann, Paris, 1932.

[8]Tumin, A. M., and Fedorov, A. V., "Spatial Growth of Disturbances in a Compressible Boundary," *Journal of Applied Mechanics and Technical Physics*, Vol. 24, No. 4, 1983, pp. 548–554.

[9]Zhigulev, V. N., and Tumin, A. M., *Origin of Turbulence*, Nauka, Novosibirsk, 1987 (in Russian); also NASA TT-20340, Oct. 1988.

[10]Tumin, A., Amitay, M., Cohen, J., and Zhou, M., "A Normal Multi-Mode Decomposition Method for Stability Experiments," *Physics of Fluids*, Vol. 8, No. 10, 1996, pp. 2777–2779.

[11]Wernz, S., and Fasel, H. F., "Numerical Investigation of Forced Transitional Wall Jets," AIAA Paper 97-2022, June 1997.

[12]Tumin, A., "Multimode Decomposition of Spatially Growing Perturbations in a Two-Dimensional Boundary Layer," *Physics of Fluids*, Vol. 15, No. 9, 2003, pp. 2525–2540.

[13]Pierce, A. D., *Acoustics*, Acoustical Society of America, New York, 1989, pp. 519–523.

[14]Wolfram, S., *The Mathematica Book*, 4th ed., Wolfram Media and Cambridge Univ. Press, New York, 1999.

H. Reed
Associate Editor